
Article:
Adamu, M and Kale, GM (2016) Novel Sol–Gel Synthesis of $MgZr_4P_6O_{24}$ Composite Solid Electrolyte and Newer Insight into the Mg^{2+}-Ion Conducting Properties Using Impedance Spectroscopy. Journal of Physical Chemistry C, 120 (32). pp. 17909-17915. ISSN 1932-7447

https://doi.org/10.1021/acs.jpcc.6b05036

Novel Sol-Gel Synthesis of $MgZr_4P_6O_{24}$ Composite Solid Electrolyte and Newer Insight into the Mg^{2+}-ion Conducting Properties using Impedance Spectroscopy

Mohammed Adamu[‡] and Girish M. Kale[‡*]

[‡]School of Chemical and Process Engineering, Institute for Materials Research, University of Leeds, West Yorkshire, Leeds LS2 9JT, United Kingdom.

Abstract

Magnesium zirconium phosphate, $MgZr_4P_6O_{24}$ (MZP) is a magnesium ion conducting ceramic material with potential for application as solid electrolyte in high temperature electrochemical sensor in non-ferrous scrap metal refining and virgin metal alloying operations. In this work, MZP was synthesised using a simple but novel and economical sol-gel route at a significantly reduced temperature. An insight into the calcination process, and possible phase transformation at higher temperature was obtained using simultaneous thermogravimetric analysis and differential scanning calorimetry (TGA/DSC). Phase identification of the synthesised material was studied after calcining the powder at 900^{o}C for 3h using X-ray diffraction (XRD); a single monoclinic phase was observed at that temperature. However, a trace amount of possible minor second phase; zirconium oxide phosphate [$Zr_2(PO_4)_2O$] was formed after heating at temperatures T ≥ 1000^{o}C. Impedance spectroscopy measurement on platinised sintered-MZP pellets were carried out in the frequency range 100 mHz – 32 MHz and in a temperature range of 30 - 800^{o}C to determine the electrical properties of MZP. Ionic conductivity of MZP was found to be equal to $7.23x10^{-3}\Omega^{-1}cm^{-1}$ at relatively lower, 725^{o}C. Furthermore, the Nyquist and modulus plots measured at 764^{o}C and 390^{o}C shows single semi-circles suggesting contribution from only grain interiors (GIs). The ion-hopping rate was calculated by fitting the conductance spectra to the power law variation, $\sigma_{ac}(\omega) = \sigma_{dc} + A\omega^n$. The ac and dc conductivity of MZP show Arrhenius-type of behaviour with activation energies in the range $0.84 \leq E_a(eV) \leq 0.87$. SEM of the fractured MZP pellet sintered at 1300^{o}C for 24h revealed a highly dense microstructure with clearly visible grain boundaries and low porosity which is in good agreement with the relative density of ~99% determined using the Archimedes' principle and the theoretical density calculated from the crystal structure. EDS confirms the presence of Mg, Zr, P, O in appropriate atomic ratio to yield $MgZr_4P_6O_{24}$. Finally, TEM on MZP particles with crystallite size of ~50nm also confirmed MZP as stable at 900^{o}C with no observable second phase, $Zr_2(PO_4)_2O$.

1. Introduction

Magnesium Zirconium Phosphate, $MgZr_4P_6O_{24}$ (MZP) is an excellent magnesium ion conductor that has potential applications as solid electrolyte in high temperature electrochemical sensors for non-ferrous scrap metal refining and virgin metal alloying operations. It is envisaged that the use of in-line chemical sensors for continuous monitoring of metallurgical processes such as scrap refining and virgin metal alloying operations is likely

* E-mail: g.m.kale@leeds.ac.uk; Tel: 0044-113-3432805

to reduce significant environmental damage by lowering the carbon footprint, reduce cost of metal production and enhance the product quality. Mg^{2+} is stable in its +2 oxidation state and has ionic radius of 57pm and 72pm with the coordination numbers, 4 and 6 of tetrahedrally and octahedrally coordinated cation respectively.[1] Furthermore, in magnesium containing phosphates such as $Mg_{0.5}M_2(PO_4)_3$ (M = Ti, Zr, Hf),[2-4] the coordination number of magnesium cations is either 4 or 6. MZP as a solid electrolyte was first investigated by Ikeda *et al.*[5] and was successfully used to develop CO_2 potentiometric sensors.[6,7] Kale *et al*.[8,9] furthered the research and employed MZP for the development of Mg-sensor for aluminium alloying and refining process. Wang and Kumar[10] investigated a SO_2 gas sensor based on MZP as a solid electrolyte and Na_2SO_4 as auxiliary electrode.

In all the earlier research work related to synthesis and characterisation of MZP, the phosphate compound has been synthesised by solid state ceramic route which is known to be highly inefficient. Furthermore, our literature review indicated that there is a considerable lack of insight into the electrical conducting property of MZP. Therefore, in this work MZP was successfully synthesised using the sol-gel method and its electrical properties were investigated in order to evaluate its possible application as a solid electrolyte in a high temperature electrochemical magnesium sensor. Advantage of synthesising ceramic materials using the sol-gel approach becomes apparent as the formation temperature is greatly reduced. This procedure yields reproducibly and consistently a pure single phase material whereas other methods may fail since mixing in sol-gel synthesis occurs at molecular level among the precursors.

2. Experimental Procedure

2.1 Materials preparation:

Fine crystalline powders of $MgCO_3$ and $ZrOCl_2.8H_2O$, aqueous HNO_3 (ACS reagent, 70%) were supplied by Sigma-Aldrich (Gillingham, Dorset, UK) and $NH_4H_2PO_4$ by Alfa Aesar (Heysham, Lancashire, UK), were weighed according to their stoichiometric amount for the synthesis of single phase $MgZr_4P_6O_{24}$.

2.1.1 Procedure:

MZP was synthesised by the modified sol-gel technique based on the procedure outlined by Mielewczyk *et al.*[11]. Aqueous solutions of $Mg(NO_3)_2$ and $NH_4H_2PO_4$ were prepared separately and mixed together while continuously stirring in a beaker with a magnetic stirrer to form the homogeneous sol. To this homogeneous sol, an appropriate amount of aqueous $ZrOCl_2.8H_2O$ solution was added dropwise through the burette. The order of mixing solutions is important to obtain a homogeneous gel. NH_4OH was thereafter added dropwise to the gel to adjust pH from its initial value of 1.2 to a final pH of 10.2. The final solution was stirred for 1h and subsequently the gel was dried at 100^{o}C for 24h on a hot plate. After drying, the resultant powder was mechanically ground with a mortar and pestle, and calcined at 900^{o}C for 3h to remove the volatiles and to yield a single phase MZP. The calcined powder was later pressed

into several pellets of 13mm Ø and 2mm thickness at 5kN load in a uniaxial steel die. These pellets were sintered at different temperature in the range of 1000-1500^{o}C and annealed for 24h in order to achieve highly dense pellets for conductivity measurement.

2.2 Characterisation techniques

A Simultaneous Thermal Analyser (STA) 8000 (PerkinElmer, Seer Green, UK) was used to study phase evolution in the dried xerogel. Simultaneous TGA/DSC experiments were conducted on MZP xerogel sample using alumina crucibles in a controlled air atmosphere at a flow rate of 50 mL min^{-1}. The TGA/DSC analyses were carried out from ambient temperature to 1000^{o}C with the heating rate maintained at 10^{o}C min^{-1} without any holding time. The measurement gave an insight into a suitable calcination temperature of the MZP xerogel as well as its thermal stability.

The powder X-ray diffraction (XRD, PANalytical X'Pert MPD, Almelo, Netherlands) was used for phase identification, transformation or evolution at both ambient and high temperatures on the MZP powder and pellets. Phase identification was carried out on calcined powders at ambient temperature whereas phase transition in xerogel powders was determined by high temperature XRD (HT-XRD) in a temperature range of 25-900^{o}C. Monochromatic CuK_{α} radiation (λ = 1.5406Å) in a continuous scan over a range 2θ = 10-80^{o} at a total time of approximately 770s with a step size of *ca.* 0.0334225^{o} and a time per step of 45.085s.

Impedance spectroscopy was carried out on sintered MZP pellets of 13mm Ø and 2mm thickness with symmetric contact electrodes made from platinum paste fired at 850^{o}C for 30mins to platinise the pellet electrodes for the determination of electrical conductivity. The frequency range of 100 mHz – 32 MHz with an excitation voltage of 100 mV, using a Solartron SI1260 impedance analyser was employed during the impedance measurement between 25-800^{o}C. During the impedance measurements, the sample pellets were spring loaded in a quartz rig. The quartz rig is housed in the Faraday cage within a horizontal tube furnace in order to prevent the induced EMF affecting impedance measurements.

The microstructure of MZP pellet samples were examined by scanning electron microscopy (SEM) using Carl Zeiss EVO MA15, Jena, GmbH and elemental analysis of prepared MZP solid electrolyte was analysed by energy-dispersive X-ray (EDS) spectroscopy using an Oxford Aztec X-Act EDS spectrometer attached to the Carl Zeiss EVO MA15. Further, SADP and EDS analysis was carried out with the aid of transmission electron microscopy (FEI Tecnai G2 TEM) to determine the presence of any possible minor phase which ordinarily could not be detected in the XRD analysis.

3. Results and discussion

3.1 TGA/DSC measurement

The simultaneous TGA/DSC measurements were aimed at predicting the progress of calcination of the dried MZP xerogel powder. The results of thermal analysis in Fig. 1 shows both the TGA and DSC curves in the temperature range 30-1000°C. The TGA curve shows the progressive weight loss of the starting xerogel during the decomposition process in a temperature range of 30-500°C. It was observed from the decomposition pathway on the graph that the sharp drop in weight is as a result of the decomposition of the component precursor materials such as $NH_4H_2PO_4$, $Mg(NO_3)_2$, $ZrOCl_2.8H_2O$ having a respective decomposition temperatures of 190°C, 330°C, 437°C, respectively to form MZP at 870°C which remains stable up to 1000°C. H_2O, NH_4Cl, HCl and HNO_3 that are by-products of the stoichiometric reaction referred to as MZP residues easily vaporise during calcination. The DSC profile shows two endothermic decomposition peaks observed at (a)190°C and (b)330°C. Exothermic peak was observed at (c)870°C and it is believed that MZP is formed at this temperature. At 190°C, $NH_4H_2PO_4$ decomposed into P_2O_5, H_2O and NH_3 while $Mg(NO_3)_2$ decomposed into MgO, NO_2 and O_2 at 330°C. Similarly, $ZrOCl_2.8H_2O$ also decomposed into ZrO_2, HCl and H_2O at 437°C. P_2O_5, MgO and ZrO_2 formed in-situ are reactive powders that yield high purity single phase MZP at approximately 870°C. The TGA profile of dried MZP xerogel powder is in good agreement with the DSC profile shown in Fig. 1. A small exothermic peak could be forming at approximately 1000°C shown in Fig. 1 as peak (d) which is probably due to the formation of zirconium oxide phosphate, $Zr_2(PO_4)_2O$, as a minor phase. However, this phase could not be confirmed due to the maximum operating set temperature limit of the STA 8000 equipment used for TGA/DSC measurement.

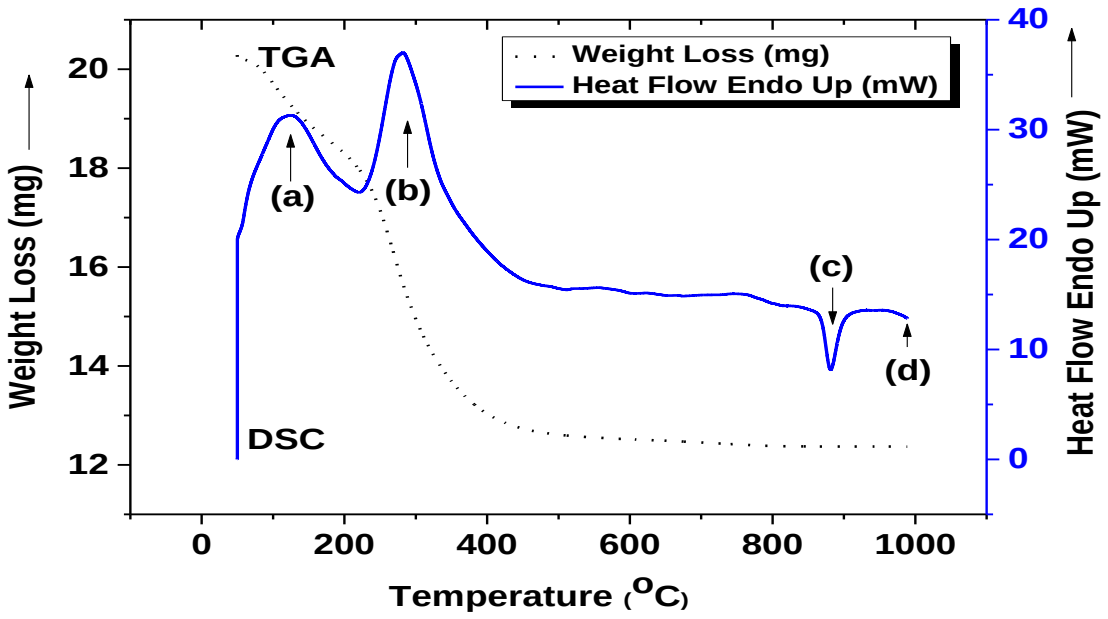

Fig. 1 TGA/DSC curves of dried precursor-gel of MZP powder, with a scan rate of 10°C min^{-1} in air.

3.2 XRD measurement

Synthesised MZP powder samples were investigated by powder X-ray diffraction to identify the phase formed. Fig. 2 reveals the X-ray diffraction pattern of a fully crystalline single phase MZP powder formed after calcining at 900^{o}C for 3h and for MZP pellet sintered at 1300^{o}C for 24h. Also analysed is MZP pellet sintered at 1090^{o}C for 1h, cooled down to 900^{o}C and annealed for 75h then compared with $Mg_{0.5}Zr_2(PO_4)_3$ and $Zr_2(PO_4)_2O$ Powder Diffraction File (PDF-Card) from the International Centre for Diffraction Data (ICDD) database. The XRD investigation for MZP pellet sintered at 1300^{o}C for 24h becomes necessary so as to ascertain whether MZP phase is well preserved after sintering at such a high temperature.

Fig. 2(a) shows that MZP is stable up to a temperature of 900^{o}C which agrees with the findings of Kazakos-Kijowski *et al.*[12] and Pet'kov *et al.*[13]. Upon sintering the MZP pellet above 1000^{o}C, a few additional minor peaks were discovered which suggested the presence of a second minor phase. The MZP pellet was also sintered at 1300^{o}C for 24h, which resulted in a highly dense pellet with the presence of a second minor phase, $Zr_2(PO_4)_2O$ as shown in Fig. 2(b).

By increasing the sintering temperature to 1470^{o}C, the additional peak became pronounced particularly at 22^{o} of 2θ which could be identified as $Zr_2(PO_4)_2O$. Although, the pellets sintered at 1470^{o}C for 24h were highly densified, the XRD measurement depicts a presence of an orthorhombic $Zr_2(PO_4)_2O$. The sintering temperature was later increased to 1500^{o}C and annealed for 24h in order to achieve a monoclinic MZP. However, it was observed that at higher temperatures, MZP completely transformed into $Zr_2(PO_4)_2O$ irrespective of annealing duration. Fig. 2(c) shows an XRD pattern for MZP pellet heated up to 1090^{o}C, showing that $Zr_2(PO_4)_2O$ was detected at this temperature. This is also in agreement with the earlier discussion of DSC trace shown in Fig. 1 at temperature higher than 870^{o}C. The pellet was then cooled down to 900^{o}C and annealed for 75h. It is proven that MZP is stable up to 900^{o}C[12] and transforms thereafter but the possibility of achieving a reversible transformation to single phase MZP is confirmed by this approach since the $Zr_2(PO_4)_2O$ characteristic peaks diminished significantly when the MZP pellet sintered at 1090^{o}C is annealed for 75h at 900^{o}C. Hence, the tendency of MZP and the minor second phase $Zr_2(PO_4)_2O$ to revert back to a single phase of MZP is possible if annealed at 900^{o}C for a prolonged period when MZP is sintered in the vicinity of 1000^{o}C considering that the loss of P_2O_5 is likely to be less and diffusion kinetics in solid state materials is likely to be slow. Hence we are led to believe that the dissociation of MZP to $Zr_2(PO_4)_2O$ occurs according to the following reaction:

$$\mathbf{MgZr_4(PO_4)_6\ (s) = 2Zr_2(PO_4)_2O\ (s) + P_2O_5\ (g) + MgO\ (s)} \qquad \mathbf{(1)}$$

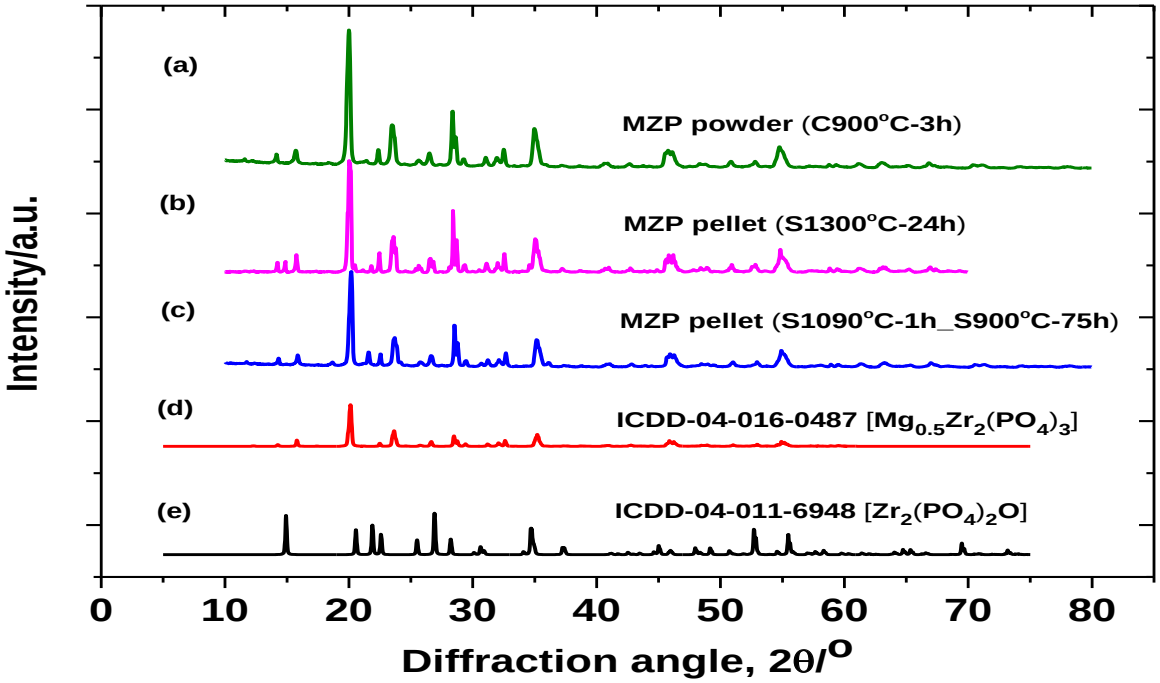

Fig. 2(a-e) XRD patterns for MZP powder calcined at 900°C for 3h and MZP pellet sintered at 1300°C for 24h; MZP pellet sintered at 1090°C for 1h, cooled down to 900°C and then annealed for 75h. Included in the stack is ICDD standard data for $Mg_{0.5}Zr_2(PO_4)_3$ and a possible second phase $Zr_2(PO_4)_2O$.

3.3 Density and porosity measurement

Fig. 3 shows the relative density of MZP samples sintered at different temperatures. Mori *et al.*[14] identified an acceptable relative density of ceramic solid electrolyte to be higher than 94%. As seen in Fig. 3, the relative density of MZP samples increases continuously from 60% to 99% as the sintering temperature increases from 1000-1300°C. The MZP samples show high sinterability, a maximum relative density of 99% of the theoretical density was achieved at a sintering temperature of 1300°C with a stable monoclinic MZP phase that satisfied the requirement for MZP solid electrolyte for sensor applications between 700°C-1100°C. Furthermore, the sintering temperatures in the range 1300-1500°C shows transformation from monoclinic MZP to orthorhombic $Zr_2(PO_4)_2O$ phase which resulted in the decrease in the relative density values from 99% to 82%. The variation of porosity of the MZP pellets as a function of the sintering temperature is also shown in Fig. 3. It can be seen clearly from Fig. 3 that the porosity of the samples decreases with increasing the sintering temperature. Especially, in the range of 1000-1300°C, the porosity decreases rapidly, which reduces from 40% to 1%. Fig. 3 shows that at the sintering temperature of 1300°C with a porosity of 1% yields the least porous and most stable MZP samples. The sintering temperatures in the range of 1300-1500°C shows increase in porosity from 1% to 18% with a crystal structure transformation from a monoclinic MZP to an orthorhombic $Zr_2(PO_4)_2O$ phase according to reaction (1). Therefore, the high volatility of P_2O_5 at higher sintering temperatures is the likely

cause of the decrease in density of MZP composite pellet suggesting that 1300°C is an optimum sintering temperature for MZP composite solid electrolyte.

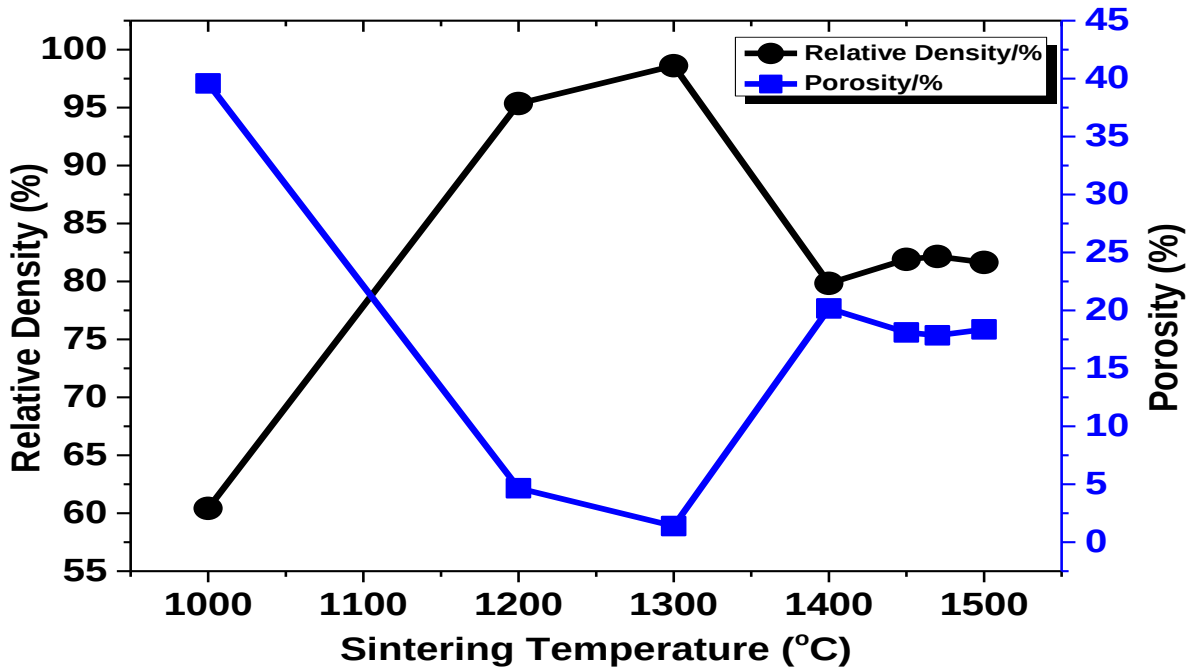

Fig. 3 The dependence of relative density and porosity of MZP solid electrolyte on sintering temperature.

3.4 Impedance spectroscopy measurement

The electrical properties of MZP composite solid electrolyte sintered at 1300°C for 24h were investigated using impedance spectroscopy. Fig. 4 shows typical impedance spectra of MZP samples sintered at 1300°C for 24h measured at 390°C and 764°C. It is noticed that only a single semi-circular response was present at both temperatures corresponding to grain interior (GI) which was consistent in the heating and cooling cycles between 30 - 800 °C.

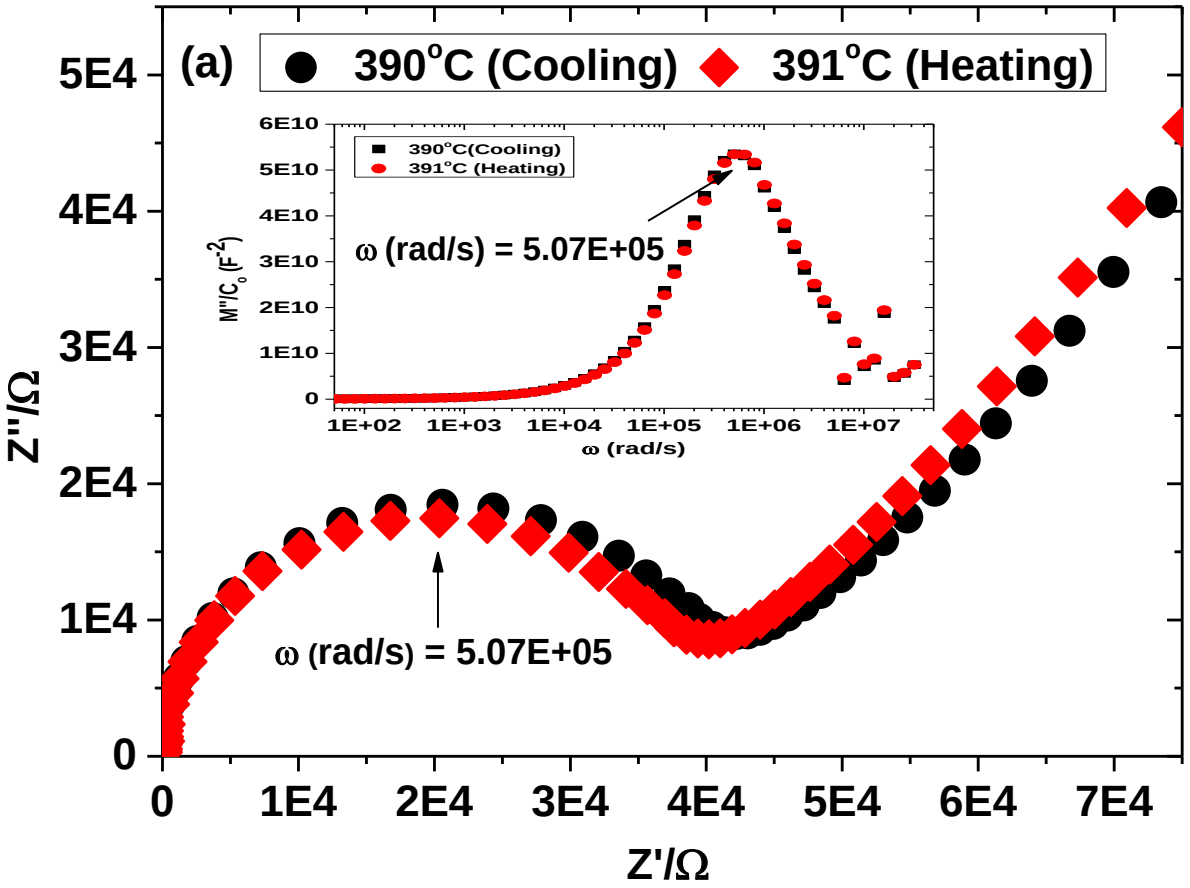
(a)
390°C (Cooling)
391°C (Heating)
ω (rad/s) = 5.07E+05
Z''/Ω
Z'/Ω
0
1E4
2E4
3E4
4E4
5E4
6E4
7E4
M''/C0 (F-2)
ω (rad/s)
1E+02
1E+03
1E+04
1E+05
1E+06
1E+07
1E10
2E10
3E10
4E10
5E10
6E10

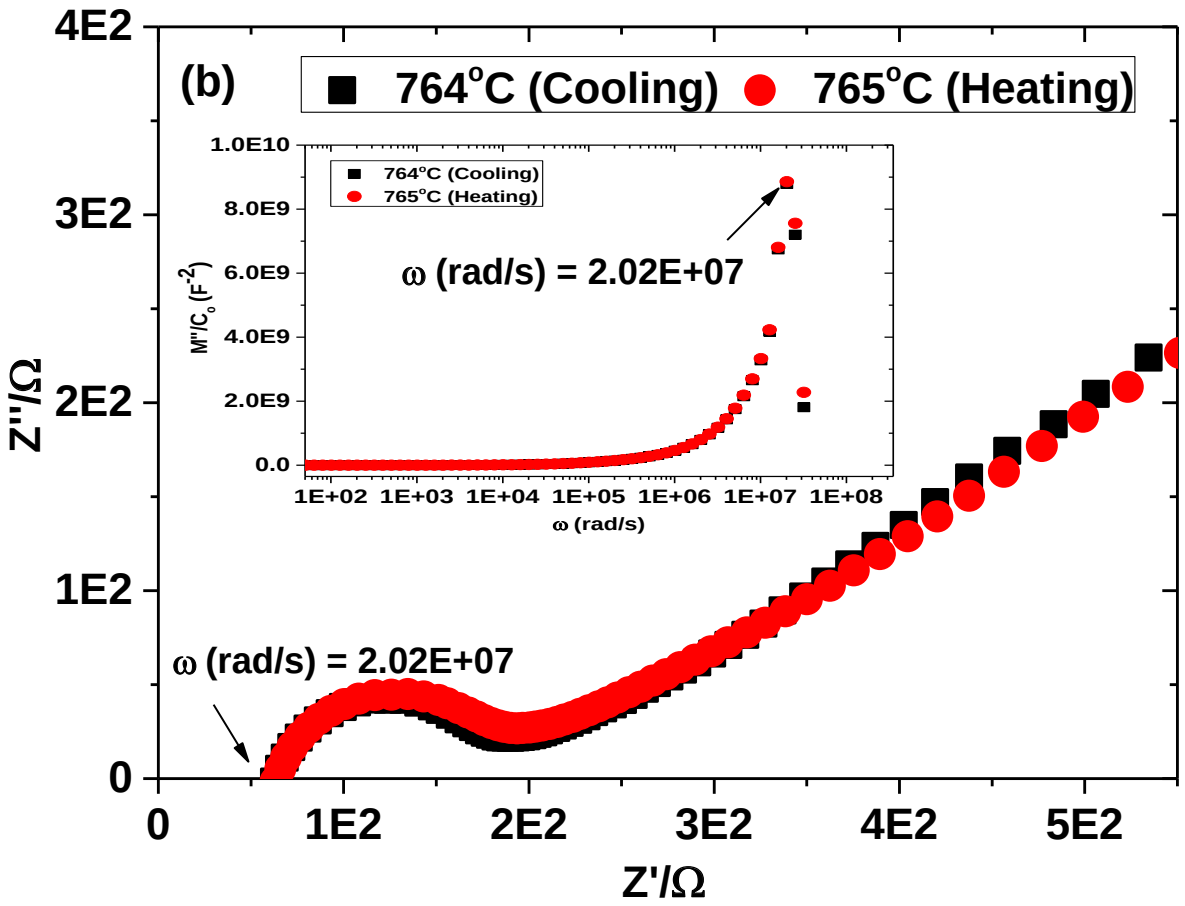

Fig. 4 The Nyquist plots of MZP pellets sintered at 1300°C for 24h measured at (a) 390°C and (b) 764°C in the frequency range of 100m Hz – 32 MHz. Insert is the electric modulus of MZP at 390°C and 764°C which shows the Nyquist plots for single relaxing species.

No feature due to grain boundaries (GB) or electrode effects (EE) was observed in this impedance spectrum which suggest a single relaxation process. Moreover, their centres are below the real axis, which indicates a non-Debye type of relaxation.[15] As temperature increases, the radius of semicircles decreases, indicating a thermally activated conduction mechanism in operation in the studied temperature range.[16] The reproducible Nyquist plots observed in Fig. 4(a) and Fig. 4(b) in heating and cooling cycle for the low and high temperature region; 391°C and 765°C, respectively, is an indication that MZP composite solid electrolyte shows reversible response which is a very important behaviour of the solid electrolytes used to design chemical sensor that is subjected to temperature variations. Fig. 4(b) shows a shift from the origin compared with Fig. 4(a) which implies that as temperature increases, the total resistance (R_t) shift towards higher values by about 50 – 70 Ω indicating that perhaps MZP composite has a slightly positive temperature coefficient of electronic resistance. The ionic conductivity of MZP solid electrolyte in this study is considerably higher than that reported elsewhere. Imanaka *et al.*[17] in their work considered MZP and other related composites as high-temperature solid electrolytes with an ionic conductivity of $6.92 \times 10^{-3} \Omega^{-1} cm^{-1}$ at 800°C. The MZP synthesised in this work shows higher ionic conductivity

of $7.23 \times 10^{-3} \Omega^{-1} cm^{-1}$ at relatively lower, 725°C. The relative density of MZP pellet obtained in this investigation is 99% against 93% obtained by Imanaka *et al.* [17]. We believe that the higher conductivity of MZP obtained in this investigation could have been highly influenced by the sol-gel preparation route employed in this study since Imanaka *et al.*[17] synthesised MZP solid electrolytes by the solid-state ceramic route which is well known for inadequate homogeneity of product phase.

The temperature dependence of the electrical conductivity of MZP sintered at 1300°C for 24h has been empirically given by equation (2) in the form of an Arrhenius equation;[18]

$$\sigma T = \sigma_o(T) \exp\left(-\frac{E_a}{kT}\right) \quad \textbf{(2)}$$

where $\sigma_o(T)$ is pre-exponential factor which is a function of charge carrier concentration, temperature and material structural parameters, k the Boltzmann constant and E_a the activation energy of conduction.

Fig. 5 shows the Arrhenius plots of the bulk conductivity of MZP sintered at 1300°C for 24h, which agrees with the relationship in equation (2). The conductivity of MZP has been found to increase with temperature. The average activation energy for ionic conduction as shown in Fig. 5 was found to be 0.84 eV. However on closer examination of the Arrhenius relationship, the lnσT versus 1000/T plot shows a significant deviation of data from linearity at ~833K which is in agreement with the results reported by Ivanov-Schitz *et al.*[19]. The deviation observed in lnσT versus 1000/T plot in Fig. 5 may be due to the transition of Mg^{2+}-ion between crystallographically different sites that influenced the conductivity at even the slightest change in ion arrangement. The activation energy, E_a = 0.84 eV is comparable with those reported by Mudenda and Kale[20] for sodium ion conductor with similar crystal structure as MZP.

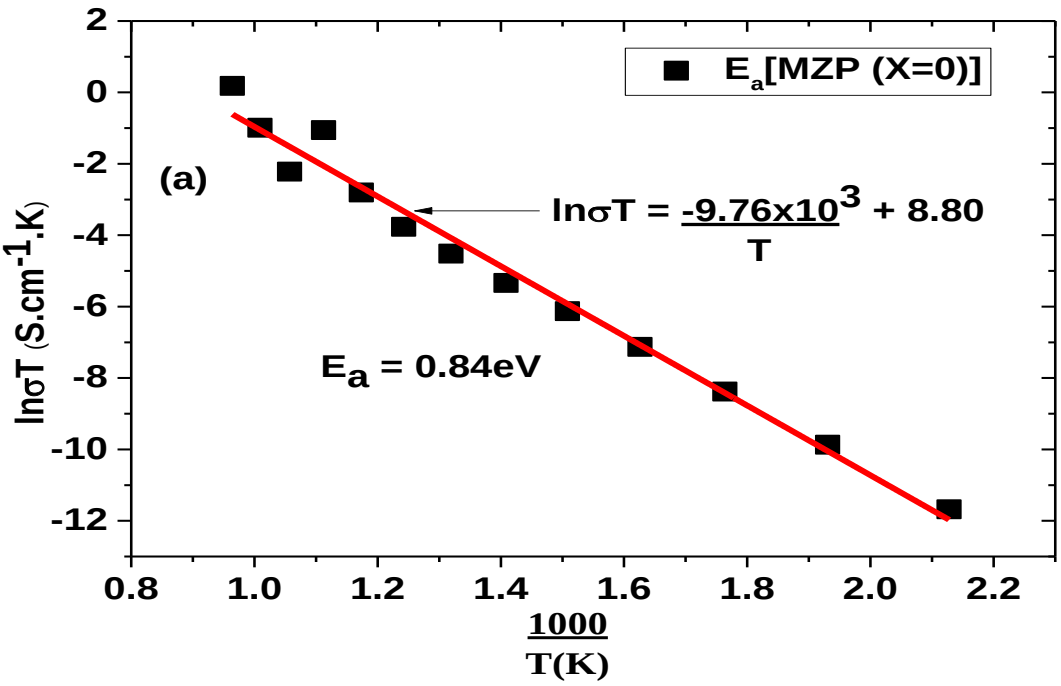

Fig. 5 Temperature dependence plot of bulk conductivity for MZP sample sintered at 1300°C.

3.5 Spectral analysis

The frequency dependence of ac-conductivity at different temperatures for MZP solid electrolyte samples sintered at 1300°C for 24h is represented in Fig. 6. It is observed that the conductivity pattern can be systematically divided into two parts. At lower frequencies, the ac-conductivity remains almost constant which corresponds to dc-conductivity while it shows dispersion with increasing angular frequency, which has a characteristic of ω^n. The dispersive region at higher frequency corresponds to the ionic or ac-conductivity. Angular frequency-dependent conductivity, σ_{ac} (ω) is well described by the Jonscher universal power law[21]

$$\sigma_{ac}(\omega) = \sigma_{dc} + A\omega^n \qquad (3)$$

and applied recently by Mudenda and Kale[20] to thick film Na^+ ion conductor where σ_{dc} is the dc-conductivity of the solid electrolyte at low frequency, A is a factor dependent on temperature and n is an exponent that is a function of temperature ($0 < n < 1$). The exponent n represents the degree of interaction between mobile ions and the environments surrounding them and it is used to suggest the appropriate model for the conduction mechanism. Three regions were observed in Fig. 6; a low frequency dispersive region, plateau and a high frequency dispersive region, respectively. The first low frequency dispersive region may be as a result of polarisation effects at the sample electrode interface (SEI). This can be explained from the view point that as frequency decreases, more and more charge accumulation takes place at the interface leading to a decrease in the number of mobile ions

which invariably lowers the conductivity. It was observed by Mariappan *et al.*[22], Govindaraj *et al.*[23] and more recently by Mudenda and Kale.[20]

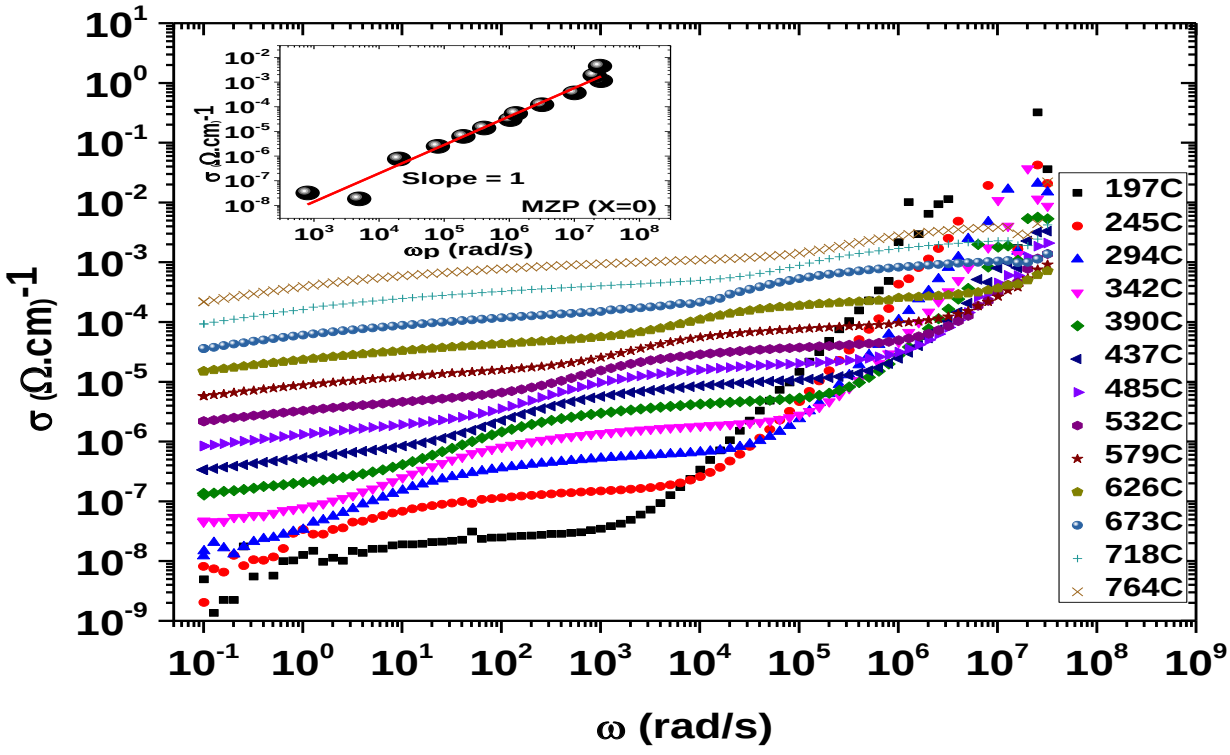

Fig. 6 Ac-Conductivity dispersion for MZP pellet. The insert is a plot of logσ vs. logω_p

Furthermore, the relaxation time could be long enough at low ω values giving adequate time for ion polarisation to take place. Since the electrode effect is more pronounced at high temperatures, this could be the reason for the spectral data curving and tending towards zero at high temperature in Fig. 6. The plateau represents the dc-conductivity and is independent of frequency. The second disperse region at high frequency [(10^4 to 10^8) Hz] represents the ac-ion-conductivity. In this region the mobility of charge carriers is high hence conductivity increases with increasing frequency. The existence of such a dispersive regime in the conductivity at higher frequencies rules out the possibility of random hopping of mobile ions and suggests that ionic motion is somehow correlated. The crossover frequency; the frequency at which ac-conductivity sets in, is temperature dependent. It can be seen from Fig. 6 that the crossover frequencies, ω_p, increase with temperature or shift towards high frequency with increase in temperature. In other words, the crossover frequency is a frequency at which transition from dc-conductivity to ac-dispersion occurs. The logarithmic plot between dc-conductivity and crossover frequency (ω_p) shown as a solid line in the plot of Fig. 6 inset gives a unit slope, which agrees with the ac-conductivity formalism[24] implying that the dc and ac conductions are closely correlated with each other and that they are of the same mechanism[25] or that the characteristic angular frequency ω_p is activated with same thermal activation energy as the dc-conductivity.[23-26]

Comparison of dc-conductivity obtained from the low frequency plateau with ac-conductivity using the Arrhenius relationship is presented in Fig. 7. The close correlation in the values implies that the conduction is from the same majority charge carrier, the Mg^{2+}, in this case. This also suggest reasonably high transference number for Mg^{2+} in MZP as well as comparable activation energy; E_a (ac) = 0.84eV and E_a (dc) = 0.87eV with some of the well-known and widely investigated cation conductors.[20]

For each temperature, the crossover frequency from dc to the dispersive region of the ac conductivity is characterised by a change in slope at a certain value of frequency which is known as hopping frequency ω_h and it can be calculated directly from ac conductivity data using the formalism described earlier by Almond and West (1983)[27]:

The hopping frequency is temperature dependent and it obeys the Arrhenius equation

$$\omega_h = \omega_o \exp\left(-\frac{E_a}{k_B T}\right) \quad (4)$$

where ω_o is the pre-exponential factor of hopping frequency and E_a the activation energy for the hopping frequency.[27] The variation of lnσT with temperature is shown in Fig. 7.

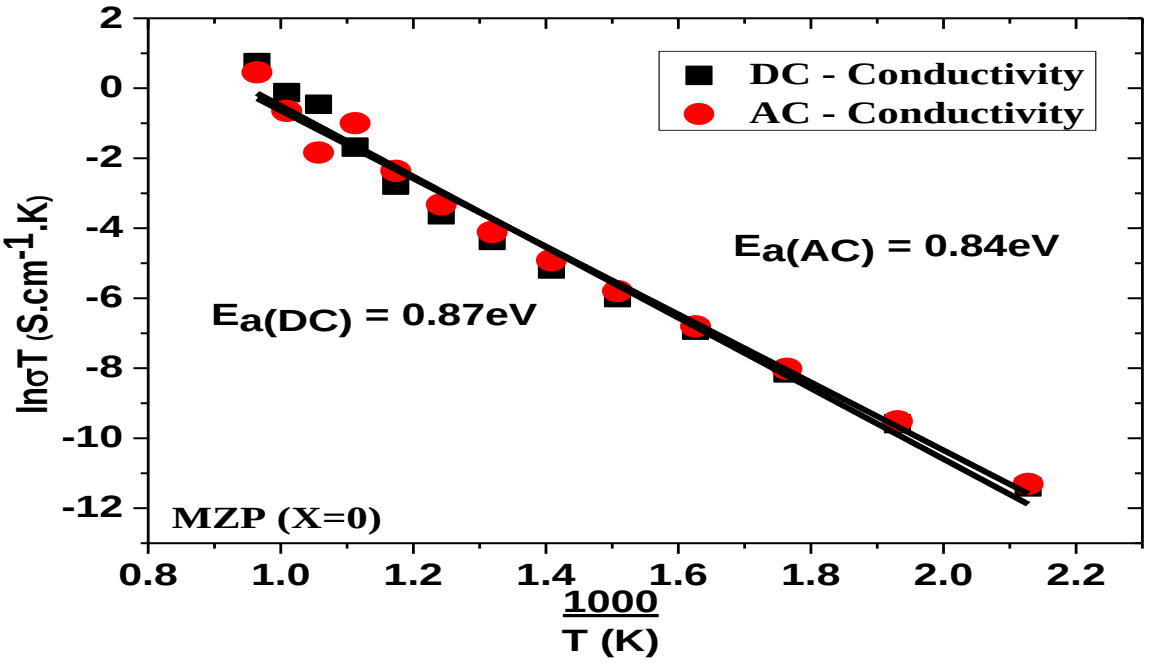

Fig. 7 Comparison of dc conductivity obtained from the low frequency plateau with ac conductivity.

According to equation (4), the activation energy calculated from linear fit of the conductivity data is 0.84eV. It is worthwhile to note that the calculated activation energy determined from dc-conductivity and that estimated from hopping frequency are in excellent agreement suggesting that the mobility of the charge carriers is due to a hopping mechanism.

3.6 SEM/EDS measurement

The SEM micrographs of a cross-section of fracture surface of sintered MZP pellet after impedance measurements and the EDS analysis of the same sample showing elemental composition of sintered MZP pellet at 1300^{o}C for 24h is presented in Fig.8. The SEM micrograph shows that the composite electrolyte pellet has high density. This is evident from the grain compact and visible grain boundaries of MZP sample sintered at 1300^{o}C for 24h. Negligible porosity was observed which is in excellent agreement with the high relative density of ~99% calculated from the measured experimental value using the pre-calibrated density bottle and the theoretical value calculated from the crystal structure of MZP. Meanwhile, EDS spectroscopy was performed on MZP pellet to analyse for the elemental composition of the solid electrolyte. The results of the EDS analysis of the MZP pellet sintered at 1300^{o}C for 24h shows the presence of Mg, Zr, P and O in appropriate atomic ratio calculated from the spectrum data presented in Fig. 8(b). The chemical compositions of MZP based on the atomic ratio confirms the formation of $MgZr_4P_6O_{24}$ within the limits of experimental uncertainty.

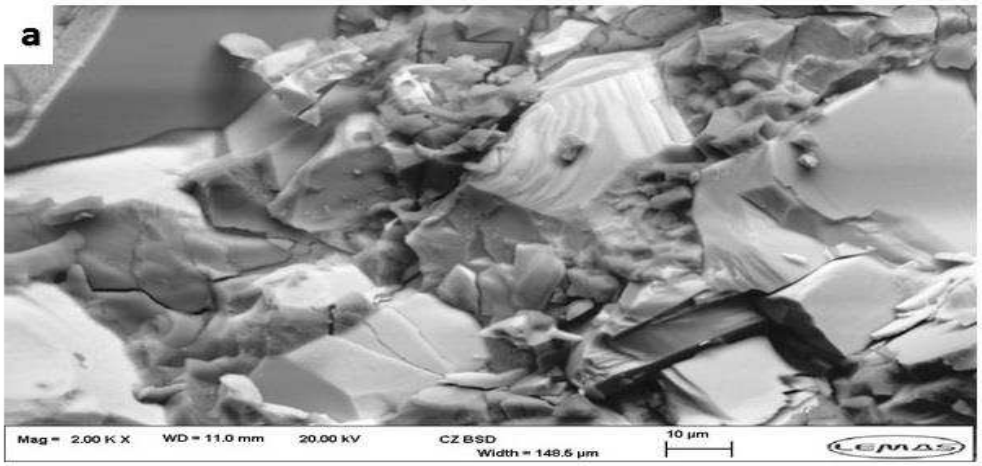

Element	Weight%	Atomic%	Atomic Ratio
Mg	2.50	2.83	1.00
Zr	38.75	11.68	4.13
P	18.62	16.53	5.84
O	40.13	68.96	24.37
Total	100.00	100.00	

Fig. 8 SEM micrographs of (a) a fractured surface $MgZr_4P_6O_{24}$ (MZP) pellet (b) EDS scan of sintered MZP pellet annealed at 1300^{o}C for 24h.

3.7 TEM measurement

The TEM micrographs of MZP powder prepared by the sol-gel method and calcined at 900^{o}C for 3h is shown in Fig. 9. The micrograph in Fig. 9(a) shows finer particles while Fig. 9(b) shows larger crystallite of the same material calcined at 900^{o}C for 3h with the same composition and crystal structure. The SADPs of Figs. 9(a) and 9(b) clearly shows very tiny (< 20 nm) amorphous and relatively larger (> 100 nm) crystalline particles, respectively.

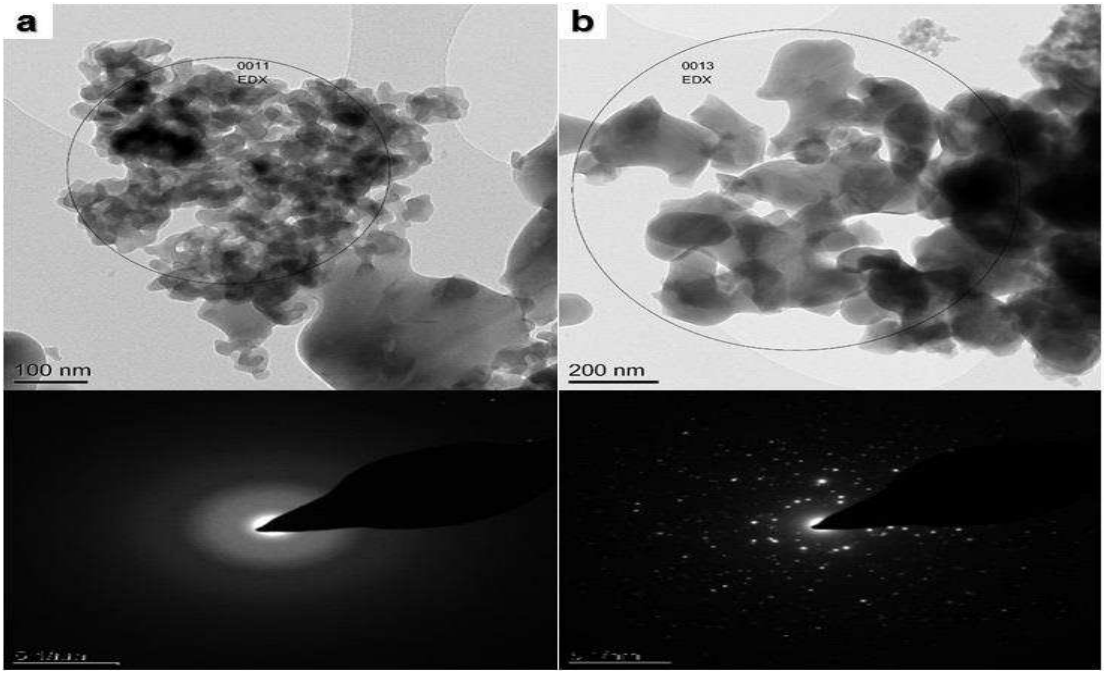

Fig. 9 TEM analysis of sol-gel derived MZP powder calcined at 900^{o}C for 3h with SADPs showing (a) amorphous and (b) crystalline particles of MZP.

4. Conclusion

Single phase MZP was successfully synthesised at relatively low temperature of 900^{o}C using a novel sol-gel method. Experimental methods such as DSC/TGA XRD, SEM, TEM and Impedance Spectroscopy (IS) were employed to characterise MZP powder and pellets to achieve a high conductivity MZP solid electrolyte for the fabrication of high temperature Mg-sensor for metal alloying and refining process control. TEM measurement on the other hand, provided a deeper insight into MZP powder calcined at 900^{o}C for 3h. The results of DSC/TGA, XRD, SEM and TEM are all internally consistent for the formation of MZP. The conductivity data of MZP reported in this article are considerably higher than those reported in the literature. The novel sol-gel route employed for the synthesis of MZP is solely responsible for the improvement in the relative density and electrical conductivity achieved in this study compared with data reported in the literature of the same material synthesised by the solid state reaction.

Acknowledgements

The authors gratefully acknowledge the funding provided by the Federal Government of Nigeria (Thru: Tertiary Education Trust Fund, TETFund) for this project. We are also thankful to the School of Chemical and Process Engineering for providing the requisite research facilities and infrastructure.

References

(1) Shannon, R. D. Revised Effective Ionic Radii and Systematic Studies of Interatomic Distances in Halides and Chalcogenides. *Acta Crystallogr., Sect. A: Cryst. Phys., Diffr., Theor. Gen. Crystallogr.* **1976,** *32*, 751-767.

(2) Barth, S.; Olazcuaga, S.; Gravereau, P.; Le Flem, G.; Hagenmuller, P. $Mg_{0.5}Ti_2(PO_4)_3$ - A New Member of the NASICON Family with Low Thermal Expansion. *Mater. Lett.* **1993**, *16*, 96-101.

(3) Pet'kov, V. I.; Kurazhkovskaya, V. S.; Orlova, A.; Spiridonova, M. L. Synthesis and Crystal Chemical Characteristics of the Structure of $M_{0.5}Zr_2(PO_4)_3$ Phosphates*. Crystallogr. Rep.* **2002**, *47*, 736-743.

(4) Orlova, A.; Artem'eva, G. Y.; Korshunov, I. Double Phosphate of Hafnium and the Alkaline-Earth Elements [Mg, Ca, Sr, Ba]*. Zh. Neorg. Khim.* **1990**,*35*, 1091-1094.

(5) Ikeda, S.; Takahashi, M.; Ishikawa, J.; Ito, K. Solid Electrolytes with Multivalent Cation Conduction. 1. Conducting Species in $MgZrPO_4$ System. *Solid State Ionics* **1987**,*23*, 125-129.

(6) Ikeda, S.; Kato, S; Nomura, K.; Ito, K.; Einaga, H.; Saito, S.; Fujita, Y. Carbon Dioxide Sensor using Solid Electrolytes with Zirconium Phosphate Framework. *Solid State Ionics* **1994**, *70*, 569-571.

(7) Ikeda, S.; Kondo, T.; Kato, S.; Ito, K.; Nomura, K.; Fujita, Y. Carbon Dioxide Sensor using Solid Electrolytes with Zirconium Phosphate Framework (2). Properties of the CO_2 Gas Sensor using $Mg_{1.15}Zr_4P_{5.7}Si_{0.3}O_{24}$ as Electrolyte. *Solid State Ionics* **1995**, *79*, 354-357.

(8) Kale, G. M.; Jacob, K. T.; Wang, L.; Hong, Y. Solid-State Electrochemical Sensor for Monitoring Mg in Al Refining Process. *The Electrochemical Society Transactions* **2006**, *1***,** 1-11.

(9) Kale, G. M. Investigation into Cation Conductors for Sensors in Aluminium Processing: $MgO_{(1+x)}Al_2O_3$, $MgZr_4(PO_4)_6$, $Li_{1.3}Al_{0.3}Ti_{0.7}P_3O_{12}$, $LiBeGeO_4$ and $Al_2(WO_4)_3$. In *International Seminar on Non-Ferrous Metals and Materials,* Jamshedpur, India, Feb 9-11, 2000; Chakrabarti, D. M., Jana, R. K., Kumar, V., Pandey, B. D., Goswami, N. G. Eds.; Steel City Press: National Metallurgical Laboratory, Jamshedpur, India, 2000.

(10) Wang, L.; Kumar, R. V. A New SO_2 Gas Sensor Based on an Mg^{2+} Conducting Solid Electrolyte. *J. Electroanal. Chem.* **2003**, *543*, 109-114.

(11) Mielewczyk, A.; Molin, S.; Gdula, K.; Jasinksi, G.; Kusz, B.; Jasinski, P.; Gazda, M. Structure and Electric Properties of Double Magnesium Zirconium Orthophosphate. *Materiały Ceramiczne* **2010**, *62*, 477-480.

(12) Kazakos-Kijowski, A.; Komarneni, S.; Agarwal, D.; Roy, R. Synthesis, Crystal Data and Thermal Stability of Magnesium Zirconium Phosphate [$MgZr_4(PO_4)_6$]. *Mater. Res. Bull.* **1988**, *23*, 1177-1184.

(13) Gobechiya, E. R.; Sukhanov, M. V.; Ret'kov, V. I.; Kabalov, Yu. K., Crystal Structure of the Double Magnesium Zirconium Orthophosphate at Temperatures of 298 and 1023 K*. Crystallogr. Rep.* **2008**, *53*, 53-59.

(14) Mori, M.; Suda, E.; Pacaud, B.; Murai, K.; Moriga, T. Effect of Components in Electrodes on Sintering Characteristics of $Ce_{0.9}Gd_{0.1}O_{1.95}$ Electrolyte in Intermediate-Temperature Solid Oxide Fuel Cells During Fabrication*. J. Power Sources* **2006**, *157*, 688-694.

(15) MacDonald, D.; McKubre, M. *Corrosion of Material. Chapter 4 Section 4.3 in Impedance Spectroscopy. Emphasizing Solid Materials and Systems, J. R. MacDonald Ed*;, John Wiley & Sons, New York, USA; 1987.

(16) Guidara, S.; Feki, H.; Abid; Y. Impedance, AC Conductivity and Electric Modulus Analysis of L-Leucine L-Leucinium Picrate. *J. Alloys Compd.* **2016**, *663*, 424-429.
(17) Imanaka, N.; Okazaki, Y; Adachi, G. Divalent Magnesium Ion Conducting Characteristics in Phosphate Based Solid Electrolyte Composites. *J. Mater. Chem.* **2000**,*10*, 1431-1435.
(18) Kilner, J.; Steele, B. C. H. *Mass Transport in Anion-Deficient Fluorite Oxides* in Nonstoichiometric Oxides, O. T. Sorensen Eds.; Academic Press, New York, 1981, 233-267.
(19) Ivanov-Schitz, A.; Bykov, A. Ionic Conductivity of the $NaZr_2(PO_4)_3$ Single Crystals. *Solid State Ionics* **1997**, *100*, 153-155.
(20) Mudenda, S.; Kale, G. M. New Insight into the Electrical Properties and Ion Dynamics of Screen Printed NASICON Thick Films. *J. Mater. Chem. A* **2015**, *3*, 12268-12275.
(21) Jonscher, A.K. The 'Universal' Dielectric Response. *Nature* **1977,** *267*, 673-679.
(22) Mariappan, C.; Govindaraj, G.; Roling, B. Lithium and Potassium Ion Conduction in $A_3TiB'P_3O_{12}$ (A= Li, K; B'= Zn, Cd) NASICON-Type Glasses. *Solid State Ionics* **2005**, *176*, 723-729.
(23) Govindaraj, G.; Mariappan, C. Synthesis, Characterization and Ion Dynamic Studies of NASICON Type Glasses. *Solid State Ionics* **2002**, *147*, 49-59.
(24) Funke, K. Jump Relaxation in Solid Electrolytes. *Prog. Solid State Chem.* **1993**, *22*, 111-195.
(25) Prakash, T. Influence of Temperature on AC Conductivity of Nanocrystalline $CuAlO_2$. *Int. Nano Lett.* **2012**, *2*, 1-3.
(26) Mariappan, C.; Govindaraja, G.; Vinoth Ratan, S.; Vijaya Prakash, G. Preparation, Characterization, Ac Conductivity and Permittivity Studies on Vitreous $M_4AlCdP_3O_{12}$ (M= Li, Na, K) System. *Mater. Sci. Eng., B* **2005**, *121*, 2-8.
(27) Almond, D.; West, A. Mobile Ion Concentrations in Solid Electrolytes From an Analysis of Ac Conductivity. *Solid State Ionics* **1983**, *9*, 277-282.